Multiple-Conformation and Protonation-State Representation in 4D-QSAR: The Neurokinin-1 Receptor System

Angelo Vedani,* Hans Briem,† Max Dobler,§ Horst Dollinger,|| and Daniel R. McMasters‡

Biographics Laboratory 3R, Missionsstrasse 60, CH-4055 Basel, Switzerland, Departments of Lead Discovery and Medicinal Chemistry, Boehringer Ingelheim Pharma, 55216 Ingelheim, Germany, and Laboratory for Organic Chemistry, ETH Zürich, 8092 Zürich, Switzerland

Received May 15, 2000

Using a 4D-QSAR approach (software *Quasar*) allowing for multiple-conformation, orientation, and protonation-state ligand representation as well as for the simulation of local induced-fit phenomena, we have validated a family of receptor surrogates for the neurokinin-1 (NK-1) receptor system. The evolution was based on a population of 500 receptor models and simulated during 40 000 crossover steps, corresponding to 80 generations. It yielded a cross-validated r^2 of 0.887 for the 50 ligands of the training set (represented by a total of 218 conformers and protomers) and a predictive r^2 of 0.834 for the 15 ligands of the test set (70 conformers and protomers). A series of five "scramble tests" (with an average predictive r^2 of −0.438) demonstrates the sensitivity of the surrogate toward the biological data, for which it should establish a QSAR. On the basis of this model, the activities of 12 new compounds − four of which have been synthesized and tested in the meantime − are predicted. For most of the NK-1 antagonists, the genetic algorithm selected a single entity − out of the up to 12 conformers or protomers − to preferably bind to the receptor surrogate. Moreover, the evolution converged at an identical protonation scheme for all NK-1 antagonists. This indicates that 4D-QSAR techniques may, indeed, reduce the bias associated with the choice of the bioactive conformation as each ligand molecule can be represented by an ensemble of conformations, orientations, and protonation states.

Introduction

The Neurokinin-1 Receptor System. The human neurokinin-1 receptor (NK1R) is one of a family of neuroreceptors involved in various signal-transduction pathways, including nociception, nausea, bronchioconstriction, vasodilation, and visceral smooth muscle contraction.[1,2] NK1R binds the undecapeptide neurotransmitter substance P (SP, Arg-Pro-Lys-Pro-Gln-Gln-Phe-Phe-Gly-Leu-Met-NH_2), discovered in 1931 by von Euler and Gaddum,[3] with a binding affinity in the 0.05−0.5 nM range.[4] Two other neurokinin receptor subclasses are known: the neurokinin-2 receptor (NK2R) and the neurokinin-3 receptor (NK3R). Historically, NK1R has been considered to be the receptor for SP, NK2R that for neurokinin A, and NK3R that for neurokinin B. However, this simple picture is complicated by the poor selectivity of the various NK receptors for the various neurotransmitters. Evidence has been presented that NK1R exists in two states: an SP-specific state and a general state which binds SP, NKA, and NKB with similar affinities.[4] A link between transmission of pain, the induction of inflammatory processes as a result of noxious stimuli, and the release of SP has been established. These observations suggest that SP receptor antagonists may be of significant therapeutic use in the treatment of a wide range of clinical conditions, ranging from arthritis, migraine, and asthma to postoperative pain and nausea.[4−6]

NK1R belongs to the class of G-protein-coupled receptors.[7] On the basis of 2D mutagenesis and fluorescence experiments,[8] the binding sites of SP and of some antagonists have been identified, as well as a number of individual residues important for binding. Together with information about the general structure of GPCRs,[9,10] low-resolution models of NK1R−antagonist complexes have been created.[11−13] While the general structure of the NK1R has been inferred based on mutagenesis, fluorescence, and binding affinity data, the low resolution inherent in these studies is not conducive to quantitative prediction of binding affinities of unknown candidates.[14]

On the other hand, the binding affinity data of a variety of NK1R antagonists has allowed the use of quantitative structure−activity relationship (QSAR) methods to predict the binding affinities of NK1R antagonists and thus accelerate the structure optimization. A recent study by Takeuchi et al. involved a constrained search of a diverse set of 72 NK1R antagonists, followed by CoMFA analysis.[5] Among the issues investigated was whether in the bioactive conformation the two aromatic groups important for binding are parallel or perpendicular to each other. While certain X-ray structures and solution data indicated that they were parallel, a different X-ray structure suggested a perpendicular arrangement. The perpendicular arrangement was found to be lower in energy and furthermore gave a better correlation than the parallel arrangement,

* To whom correspondence should be addressed. Phone: +41-61-321-0533. Fax: +41-61-321-0540. Internet: www.biograf.ch.
† Department of Lead Discovery, Boehringer Ingelheim Pharma.
§ ETH Zürich.
|| Department of Medicinal Chemistry, Boehringer Ingelheim Pharma.
‡ Present address: Merck Research Laboratories, West Point, PA 19486.

10.1021/jm000986n CCC: $19.00
Published on Web 11/01/2000

both for the training set (a cross-validated r^2 of 0.70 vs 0.57) and for an external test set (a predictive r^2 of 0.82 vs 0.78).

An experimental study by Sisto et al. identified a parallel arrangement.[15] This was corroborated by a linear correlation between the photochemical parameters (extinction coefficient and fluorescence quantum yield) of the ligands and their biological activities, where the parallel stacked configuration responsible for higher extinction coefficients and lower fluorescence quantum yields corresponded to higher activities. Horwell et al. generated structure−activity relationships (SARs) for a series of peptidic NK1R antagonists and found descriptors such as the surface area, log P, log P^2, the total dipole moment, and the number of methyl groups to be predictive for binding affinity.[16]

Quantitative Structure−Activity Relationships. QSAR is an area of computational research which builds atomistic or virtual models to predict quantities such as the binding affinity, toxicity, or pharmacokinetic parameters of a given molecule. The idea behind QSAR is that structural features can be correlated with biological activity. Of particular interest for the biomedical research is QSAR based on 3D models because they allow for the simulation of directional forces: hydrogen bonds, metal−ligand contacts, polarization effects, and interaction between electric dipoles. Such forces are known to play a key role for both molecular recognition and selective ligand binding.

In contrast to the true biological receptor − where only one ligand molecule can bind at the time − a QSAR study is typically based on a series of ligand molecules binding "simultaneously" to an averaged receptor model. This may lead to *functional-group obscuring*, an alignment of the ligands (mirroring the pharmacophore hypothesis) where important functional groups of different molecules occupy identical portions in 3D space. For example, the $-OCH_3$ substituent of one ligand might lie on top of the −OH group of another molecule. When constructing an atomistic surrogate (e.g. a pseudoreceptor model[17,18]), such a 3D arrangement will hardly permit any H-bond donor or acceptor group to approach the −OH functionality and to establish a hydrogen bond. To remove this problem, we have devised a procedure referred to as *receptor-mediated ligand alignment*.[19] Still, two shortcomings remain associated with atomistic and receptor-surface models based on averaged receptor entities: receptor−ligand adaptation (the adaptation of the shape of the binding site by means of induced fit) and H-bond flip-flop. If the ligand−receptor interaction energy is determined toward an averaged receptor model, subtle effects associated with the adaptation of the receptor to the individual ligand molecules remain unaddressed. In addition, amino acid residues at a biological receptor, bearing a conformationally flexible H-bond donor or acceptor (Ser, Thr, Tyr, Cys, His, Asn, and Gln residues) can engage in differently directed H-bonds with dissimilar ligand molecules − an effect that can also not be simulated with an averaged receptor, simultaneously binding a series of ligand molecules in a virtual experiment. Inhibitor-dependent H-bond flip-flop has been observed, for example, in the enzyme purine nucleoside phosphorylase.[20]

A more fundamental problem in QSAR is associated with the mutual alignment of the ligand molecules, i.e. the choice of the bioactive conformation. Typically, this entity is found by conformational-search protocols combined with cluster-analyzing algorithms (see, for example, refs 21, 22) without direct means to control the result. If the construction of a pseudoreceptor or a receptor-surface model is based on incorrect bioactive conformations, the resulting surrogate is hardly of any use for predictive purposes. Of course, a variety of tools have been developed to detect such erroneous prerequisites. While the alignment problem has long been recognized,[21−23] only the more recently developed 4D-QSAR technologies would seem to provide decent solutions.[24−29]

Methods

A receptor-surface model represents a high level of model abstraction. Here, the essential information about the hypothetical receptor site is provided by means of a 3D envelope, which surrounds the ligand molecules of the training set at the van der Waals distance and is populated with properties mapped onto its surface. The shape of the surface represents information about the steric nature of the receptor site; the associated properties represent other information of interest, such as hydrophobicity, partial charge, electrostatic potential, and hydrogen-bonding propensity.[30] Various algorithms to generate and validate receptor-surface models have been described.[31−33] Other significant approaches include the construction of 3D models using a 4D formalism,[24] the use of a genetic neural network,[25] and the *Catalyst* concept[26,34] as well as the utilization of self-organizing molecular-field analysis.[35]

A "quasi-atomistic receptor model" refers to a 3D receptor surface, populated with atomistic properties (hydrogen bonds, salt bridges, hydrophobic particles, virtual solvent) mapped onto it. The *Quasar* software is based on a true 4D-QSAR concept: the fourth dimension being the possibility to represent each molecule by an ensemble of conformations, orientations, and/or protonation states throughout the entire simulation, thereby reducing the bias associated with the choice of the bioactive conformation and the ligand alignment. In contrast to most other approaches in the field, our concept allows also for the simulation of local induced fit and H-bond flip-flop. The technical details of the construction of a family of receptor models in *Quasar* are published elsewhere[27−29] and shall only be summarized here:

1. Construction of Receptor Envelopes. Induced fit may be simulated by adapting a van der Waals surface (constructed about all ligands of the training set) to the topology of each ligand molecule to be used in the QSAR. This is achieved by mapping this surface on to a transiently generated inner envelope, which snugly accommodates the individual ligand molecule. This procedure − mimicking a local induced fit − can be performed isotropic (linear) or anisotropic (field-scaled).[36] The rms deviation from the van der Waals envelope is used to estimate the energy associated with the envelope adaptation. For model evaluation during the simulated evolution, this energy contributes to the total energy balance (cf. eq 1, below). As the magnitude of induced fit cannot be estimated in the absence of the true biological receptor, it is typically necessary to perform several runs differing in mode and magnitude of the induced fit.[37]

2. Generation of an Initial Family of Parent Structures. Points on the receptor surface are then randomly populated with atomistic properties (Table 1), optionally observing standard distances (2.4−3.2 Å) between H-bonding particles. While the distributed properties are identical for all ligand molecules, their exact location on the envelope varies slightly (rms fluctuations range from 0.2 to 0.8 Å with maximal individual shifts up to 2.5 Å) depending on the chosen induced fit. If there is experimental or other evidence for a solvent-accessible receptor cavity, parts of the envelope may be

Table 1. Properties of Receptor-Surface Particles Used in *Quasar*

particle (property)	nonbonded potential type[a]	electric charge	well depth of nonbonded function (kcal/mol)
hydrophobic, neutral	6/12	−	−0.024[b]
hydrophobic, positive	6/12 + electrostatics	+0.10	−0.09[b]
hydrophobic, negative	6/12 + electrostatics	−0.10	−0.09[b]
H-bond donor	10/12	−	−5.0/−4.1/−2.3[c]
H-bond acceptor	10/12	−	−5.0/−4.1/−2.3[c]
salt bridge, positive	10/12 + electrostatics	+0.25	−5.0/−4.1/−2.3[c]
salt bridge, negative	10/12 + electrostatics	−0.25	−5.0/−4.1/−2.3[c]
H-bond flip-flop[d]	10/12	−	−5.0/−4.1/−2.3[c]
surface solvent	symmetric 10/12[e]	−	−0.97/−0.80/−0.46[c,f]
void (shallow pockets)	−	−	−

[a] The values *i,j* refer to the attractive and repulsive coefficients of the nonbonded potential function used for the ligand−receptor interaction. The general form of this potential is: $E(r) = A/r^i - C/r^j$. [b] This function adapts the form $E(r) = A/r^{12} - C/r^6$. The coefficients A and C are calculated according to $A = -\epsilon(r_i + r_j)^{12}$ and $C = -2\epsilon(r_i + r_j)^6$, respectively, and with $\epsilon = (\epsilon_i\epsilon_j)^{1/2}$. The given figure represents ϵ_j; r_i and r_j correspond to the van der Waals radii of the two involved atoms. [c] Values for −O−H···Y, >N−H···Y, and −S−H···Y H-bond interactions, respectively, where "Y" denotes a virtual H-bond acceptor. Identical values are used for the X···O, X···N, and X···S arrangement where "X" denotes a virtual H-bond donor. [d] H-Bond flip-flop particles can adapt their property (H-bond donor or acceptor) to each ligand molecule within the pharmacophore, depending on its interacting functional group. [e] To avoid repulsive forces between surface solvent and any ligand molecule, a symmetric 10/12 potential (mirrored at $r = r°$) is used. This represents a possible approximation to a mobile solvent. [f] As the virtual particles are different in radius than a water molecule, the associated energy must be corrected for different volumes: $E = (2r_{vp}/2.75)^3E°$; e.g. for $r_{vp} = 0.8$ Å → $E = 0.197E°$. The 2.75 Å corresponds to a mean O−H···O H-bond distance.

assigned to represent solvent. Alternatively, regions may be defined as being purely hydrophobic in nature or nonexistent (void), allowing for shallow binding pockets. Such assignments can be static in nature or dynamically evolved.[28−29]

3. Evolution of a Model Family. Using a genetic algorithm (for a detailed description, see, for example, refs 32, 38), the initial family of receptor models is evolved simulating crossover events. At each crossover step, there is a small probability (typically 0.01−0.03) of a transcription error, which is expressed by a random mutation. Thereafter, those two individuals of the population with the highest *lack-of-fit* (rms of $\Delta G°_{pred} - \Delta G°_{exp}$ obtained from a cross-validation, augmented by a penalty for the total number and types of properties, the difference between any other model, and the selectivity within the provided ensemble of conformations, orientations, and/or protonation states) are discarded. This process is repeated until a target cross-validated r^2 (typically 0.85−0.95) or the limiting number of crossover steps is reached.

4. Estimation of Relative Free Energies of Ligand Binding. In our concept,[27−29] we have combined the approach of Blaney et al.[39] with a method of Still et al.[40] for estimating ligand solvation energies and a term to correct for the loss of entropy upon receptor binding following Searle and Williams:[41]

$$E_{bdg} \approx E_{lig-rec} - T\Delta S_{bdg} - E_{solv,lig} - \Delta E_{int,lig} - E_{env\ adapt,lig} \quad (1)$$

where $E_{lig-rec}$ represents the force-field energy of the ligand−receptor interaction;[27,42,43] $T\Delta S_{bdg}$ the change in ligand entropy upon receptor binding;[41] $E_{solv,lig}$ the ligand desolvation energy;[40] $\Delta E_{int,lig}$ the change in ligand internal energy upon receptor binding; $E_{env\ adapt,lig}$ the energy uptake required for modifying the averaged receptor envelope (cf. above).

When using a multiple-ligand representation, the interactions of all conformations, orientations, and protonation states are calculated toward all members of the receptor-model family. The contribution of an individual entity to the total energy is determined using a normalized Boltzmann distribution:[27,28]

$$E_{bdg,tot} = \Sigma E_{bdg,ind} \exp(-w_i E_{bdg,ind}/E_{bdg,ind,lowest}) \quad (2)$$

where $w_i = (\Sigma E_{bdg,ind}/E_{bdg,ind,lowest})^{-1}$ is the normalizing factor.

Free energies of ligand binding, $\Delta G°_{prd}$, are then predicted by means of a linear regression between $\Delta G°_{exp}$ and E_{bdg} (cf. eq 1) using the ligand molecules of the training set:

$$\Delta G°_{prd} = |a|\ E_{bdg} + b \quad (3)$$

Slope and intercept of eq 3 are inherent to a given receptor model and are subsequently applied to predict the relative binding energy of ligand molecules different from those in the training set. In contrast to other methods, we calibrate each receptor system with a training set,[27−29,19] rather than apply an universal function for the various receptor systems.

5. Analysis of the Model Family. A mandatory criterion to validate a family of receptor models is their ability to predict relative free energies of ligand binding for an external set of test ligand molecules, not used during model construction (e.g. its rms deviation or the predictive r^2 value). A more serious challenge to a model family is the so-called *scramble test* (cf. ref 38). Here, the binding data (i.e. $\Delta G°_{exp}$) of the training set are randomly scrambled with respect to the true biological values, and the simulation is repeated under otherwise identical conditions. If, under these circumstances, the ligands of the test set are still predicted correctly (i.e. a predictive $r^2 > 0.5$), the model is worthless, as it is not sensitive to the biological data ($\Delta G°_{exp}$) used to establish the QSAR. The ultimate test, however, is the prediction and experimental verification of the activity of new compounds (cf. below).

Results and Discussion

The NK1R represents an attractive biological system for the more recently developed 4D-QSAR technology[27−29] as the included antagonist molecules not only feature conformational flexibility and span 4 orders of magnitude in binding affinity but also include two protonable N atoms (a piperazyl or two piperidyl moieties). Moreover, all experimental data have been obtained by a single laboratory at Boehringer Ingelheim (Germany)[44] and can, therefore, be more safely compared than a collection of literature data would allow.

The 65 NK-1 antagonists used in this study represent a series of aromatic amide derivatives which display specific affinity for NK1R. This series is built around a framework including two aromatic groups, linked by an amide moiety (Figure 1). Attached to this scaffold are cyclohexyl, piperadinyl, or piperazinyl rings. While one aromatic group consists of most of the derivatives of the 3,5-bis(trifluoromethyl)phenyl ring, the substitution at the second aromatic ring is highly varied (Figure 2).

First, a conformational search was performed on the monocationic ligands using a Monte Carlo method[45] as implemented in *MacroModel* 6.5.[46] The energy cutoff for seeding was set at 6 kcal/mol, and all conformers within 25 kcal/mol of the global minimum were saved. The structures were minimized to a gradient of 0.05 kcal/

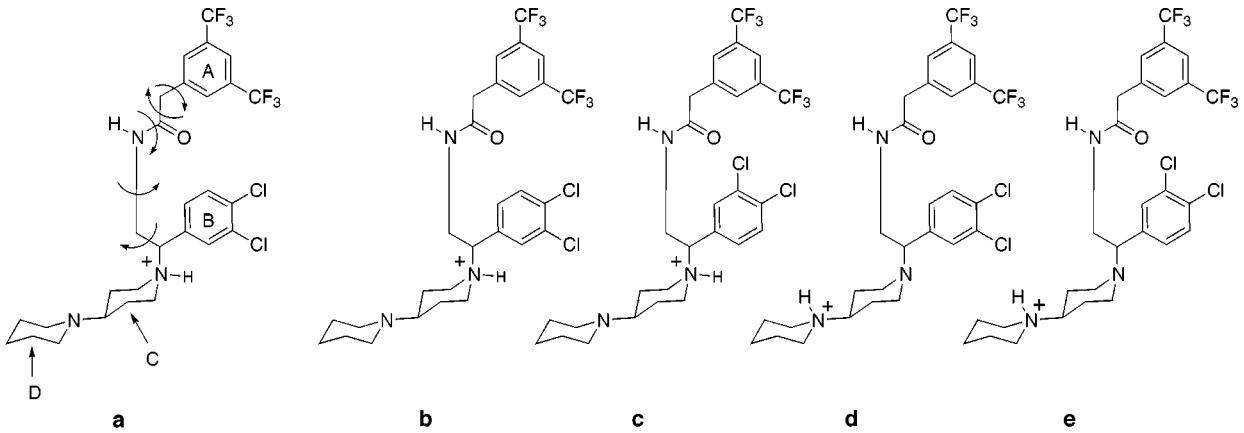

Figure 1. Conformer and protomer selection within the NK-1 data set: a, definition of the backbone torsion angles; b−e, conformations of ligand **M09** selected in this 4D-QSAR study.

(Å·mol) using a truncated Newton conjugate gradient,[47] combined with the AMBER force field[48] and implicit aqueous solvent.[40] Unique final structures were subjected to full minimization to low gradient. Due to the large number of variable torsions (11−17), none of the ligands conformational space could be exhaustively sampled − up to 10 000 conformers per ligand were identified. Although there is no limitation in *Quasar* for the number of different conformations, orientations, and protonation states of a ligand molecule, the induced-fit simulation may lead to unrealistic results if a too diverse data set is used.[28]

For analyzing the Monte Carlo conformational-search output, five adjacent torsional angles defining the scaffold were used (Figure 1). For each conformer of each compound, those torsions defining a "common backbone conformation" were evaluated (with the exception of compounds **M12**, for which the common atoms are not contiguous, and **M29**, for which they are not uniquely defined). Next, the lowest-energy conformer adopting a common conformation (defined by these five torsional angles) was selected for each compound and its energy above the global minimum was evaluated. For each backbone arrangement, this yielded a set of 65 (the total number of training and test compounds) conformations. Examination of these ensembles of backbone conformations revealed that most of them shared the same conformation in ring C, despite the fact that the ring-C conformation was not part of the backbone definition. The preferred puckering and orientation of ring D observed in most of these molecules was determined and subsequently used for all molecules. For those ligands in which the ring-D orientation was different, the orientation used was between 0.1 and 0.8 kcal/mol higher in energy. The conformers used for the final alignment lie between 0.0 and 4.9 kcal/mol above the global minimum.

Next, partial charge models were calculated using the ESP algorithm[49] (as implemented in MOPAC 6.0[50,51]) with the MNDO wave function.[52] Solvation energies were determined with the GB/SA algorithm[40] using *MacroModel* 6.5.[46] Relative energies of the various ligand conformers were determined with the AMBER force field after minimization with implicit aqueous solvent. For each asymmetrically substituted aromatic ring (A and B), two separate conformations were generated by rotating the ring by 180°. In the case of two such rings, four conformers were generated. Methoxy and isopropoxy groups were also rotated by 180° to yield two different conformations. In the case of compound **M29**, rotation around the diphenyl−carbonyl bond gave three different positions of the diphenyl group. In all, between one and six conformers were included. Additionally, two different protonation states were generated by protonating two amine functions of each ligand, with the exception of ligands **M1**, **M12**, and **M19**, which all have a single protonable amine each. This yielded a total of 288 conformers/protomers for the 65 NK-1 antagonists. Partial charges, solvation energy, and ligand internal energies were recalculated for each conformer/protonation state. The internal energy was taken relative to the lowest-energy conformer (from the Monte Carlo search) of all entities with the same protonation state. The corresponding ensemble of compound **M09** is shown in Figure 1. A training set comprising 50 molecules (218 conformers and protomers total) was then selected representing the largest possible diversity from the whole data set. The remaining 15 ligands (70 conformers/protomers total) were defined as the test set.

The mean envelope was generated using all ligands but **M12**, **M13**, **X26**, and **X30** which feature a cyclic amide and display a relatively low affinity.[53] The individual envelopes of the 65 ligands of the data set were then generated using a field-based, anisotropic algorithm.[27−29,36] The resulting "induced fit" ranged from 0.9 to 1.6 Å with associated energies of 0.8−2.7 kcal/mol. Using an initial population of 500 receptor models and a transcription-error rate set to 0.02, the system was allowed to evolve for 40 000 crossover cycles, corresponding to 80 generations. The simulation reached a cross-validated r^2 of 0.887 and a predictive r^2 of 0.834. These quantities reflect values averaged over the 500 models, which, among themselves, differ in 22−32% of the mapped 319 properties. The cross-validation was based on five groups comprising 10 ligands (leave-10-out). A stereo representation of the receptor surrogate is depicted in Figure 3; experimental and calculated IC_{50} values are compared in Table 2; a graphical comparison is shown in Figure 4.

The rms deviation for the 50 ligand molecules of the training set of 0.37 kcal/mol corresponds to an uncertainty factor of 1.9 in the IC_{50} and the maximal individual deviation (compound **M9M**, 1.1 kcal/mol) to a factor 7.1 in the IC_{50}. The corresponding rms for the

M09 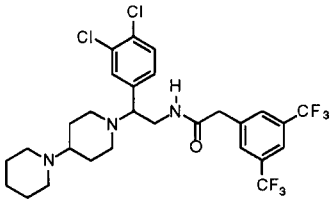	**X34** 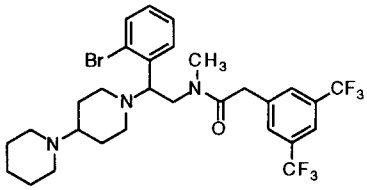	**X28** 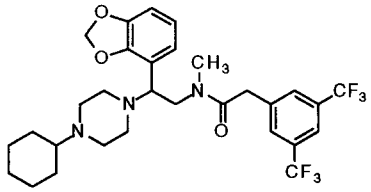
M28 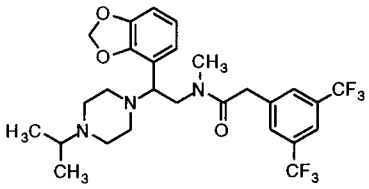	**X04** 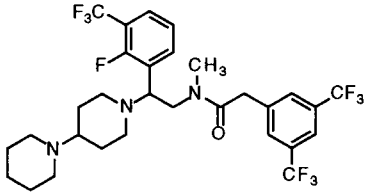	**X05** 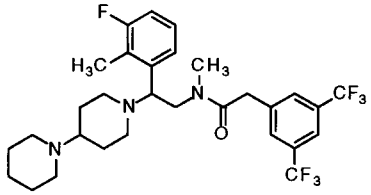
X11 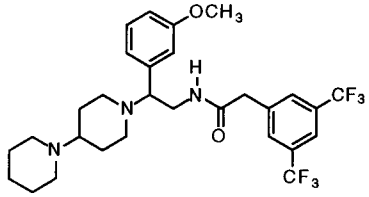	**M22** 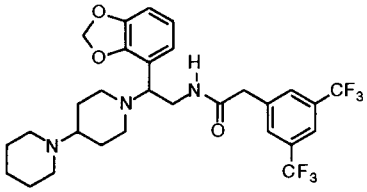	**X27** 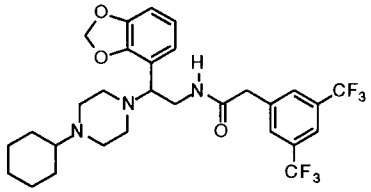
X06 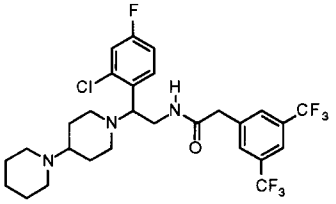	**M24** 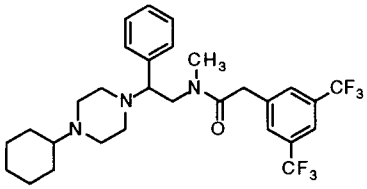	**M21** 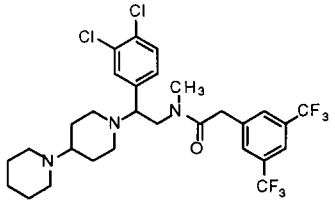
M08 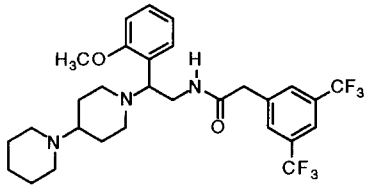	**M15** 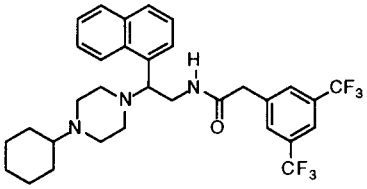	**M26** 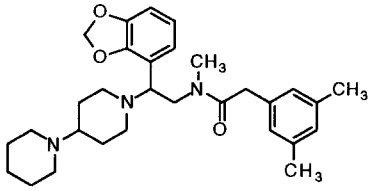
X07 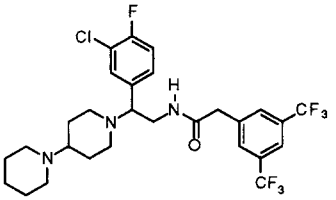	**M23** 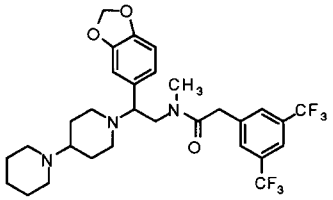	**M11** 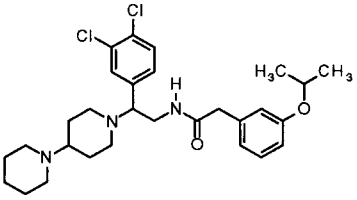
X31 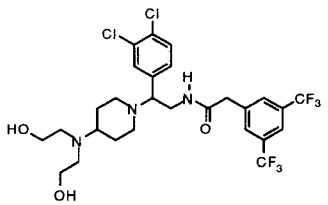	**M25** 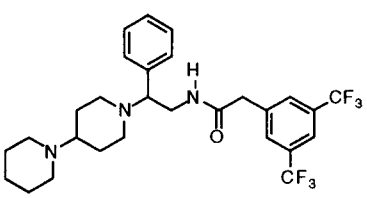	**X23** 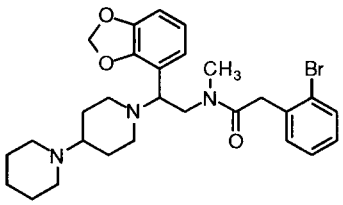

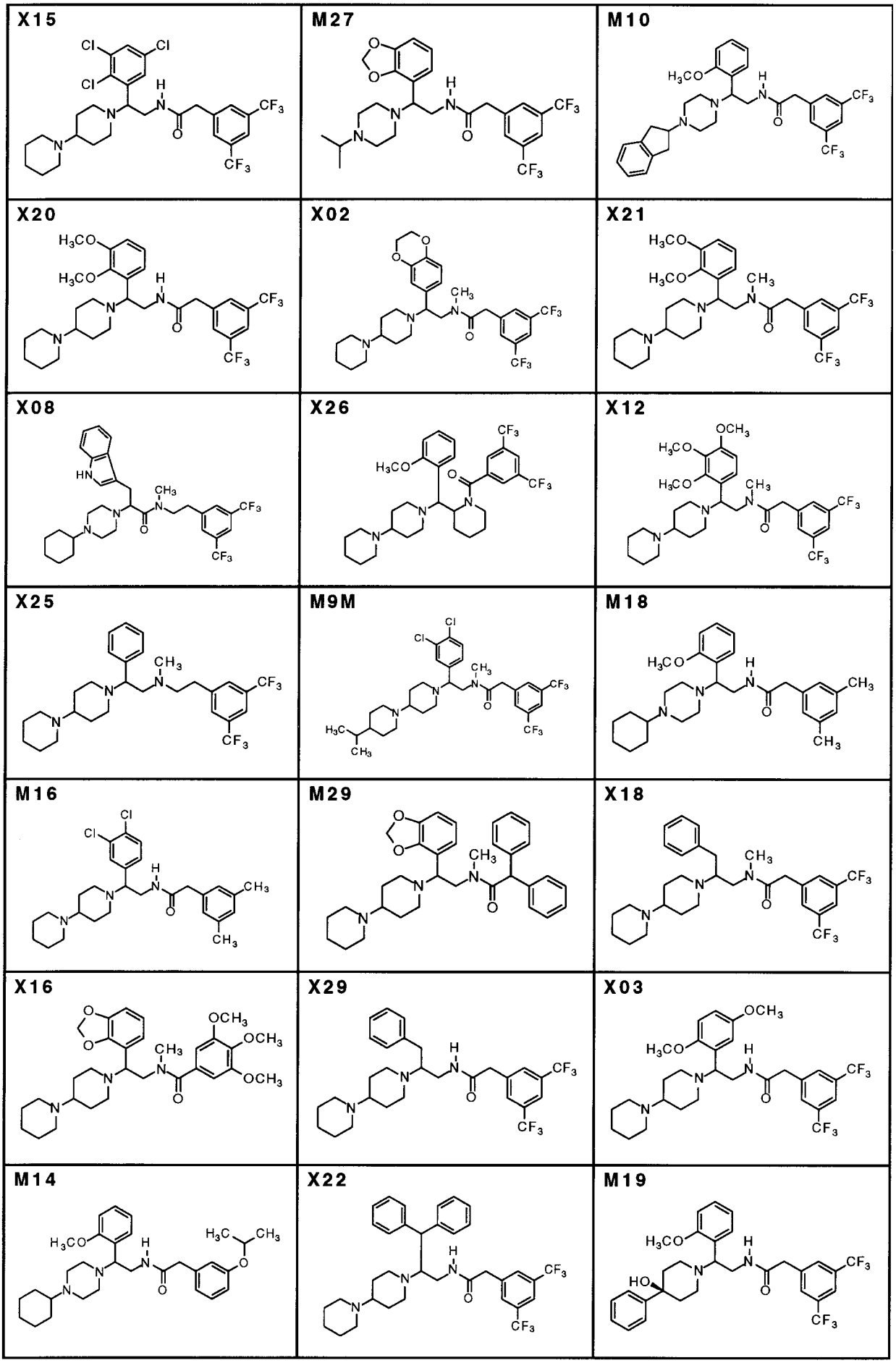
X15
M27
M10
X20
X02
X21
X08
X26
X12
X25
M9M
M18
M16
M29
X18
X16
X29
X03
M14
X22
M19

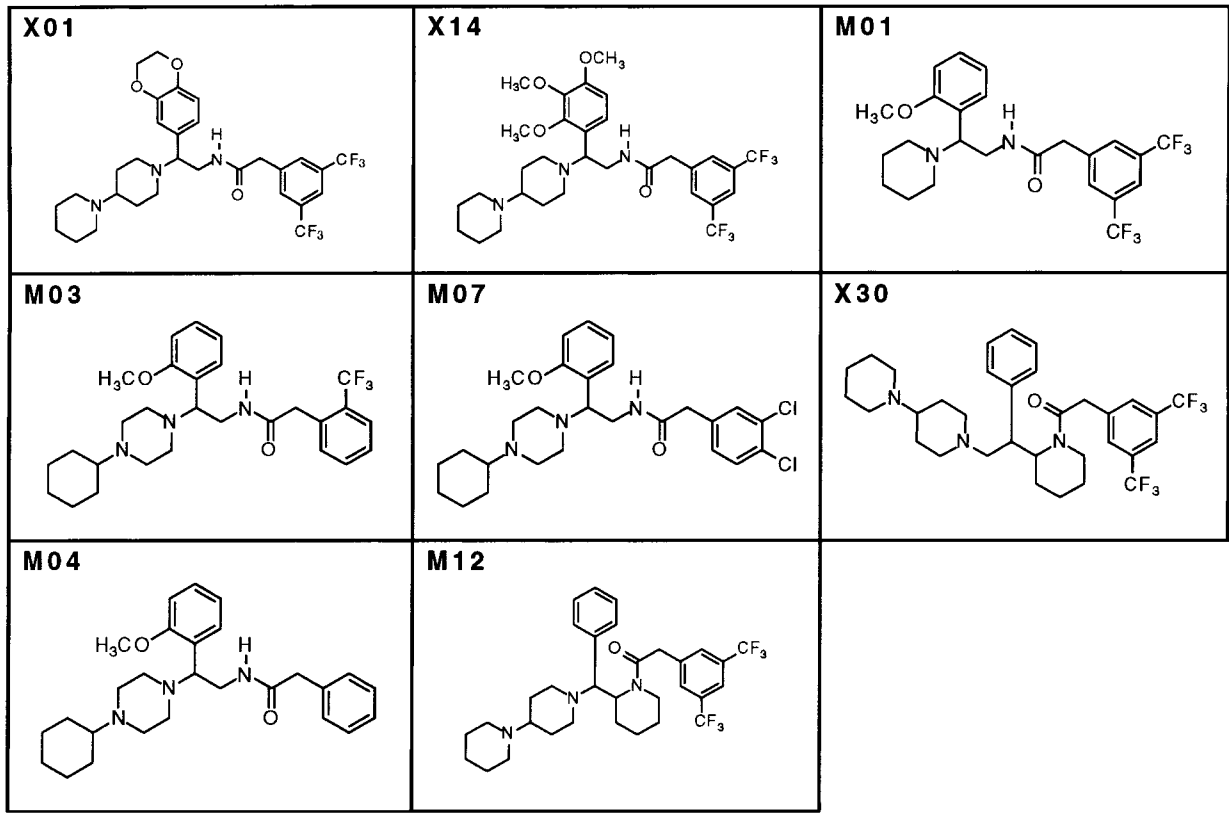
X01
X14
M01
M03
M07
X30
M04
M12

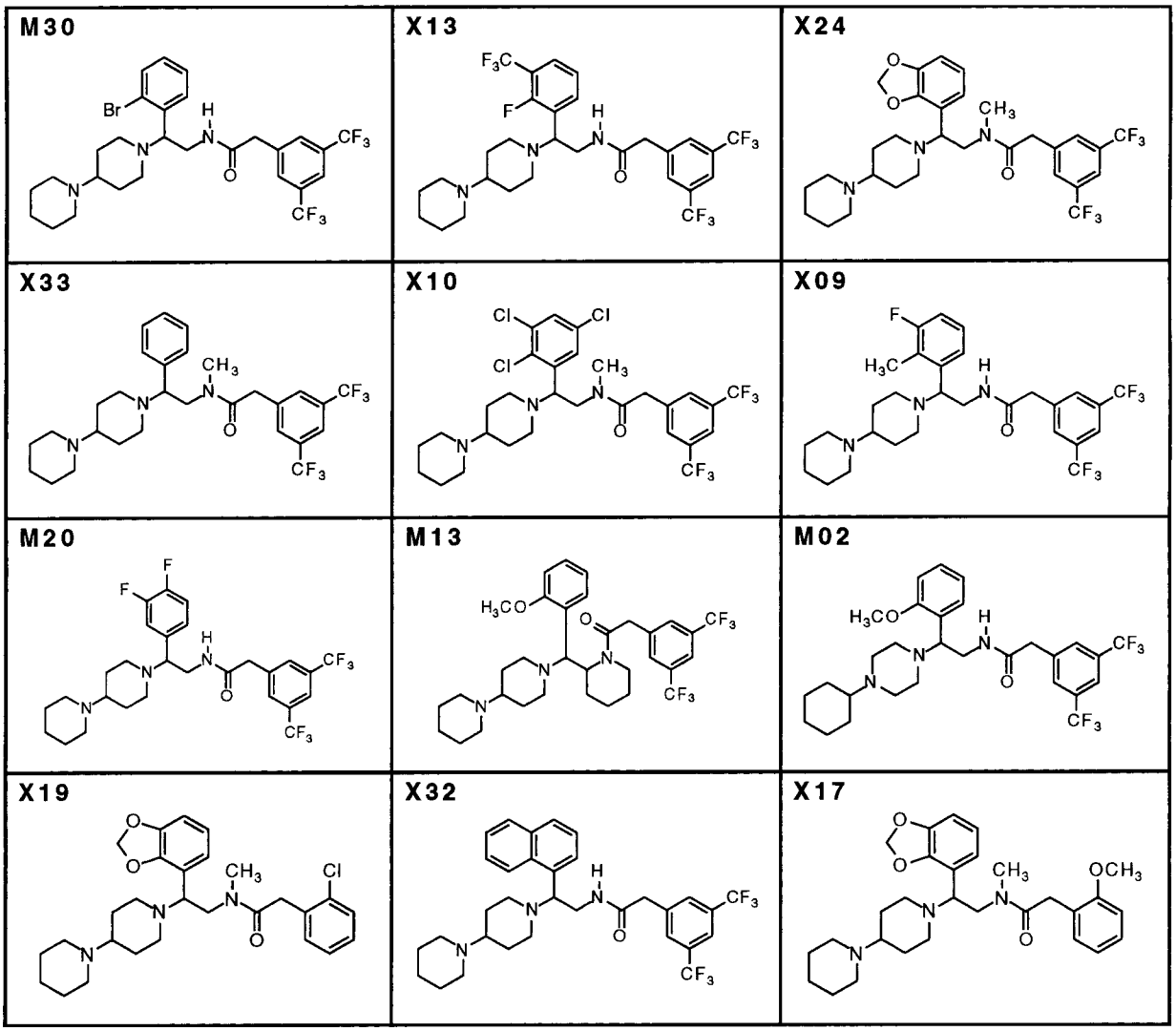
M30
X13
X24
X33
X10
X09
M20
M13
M02
X19
X32
X17

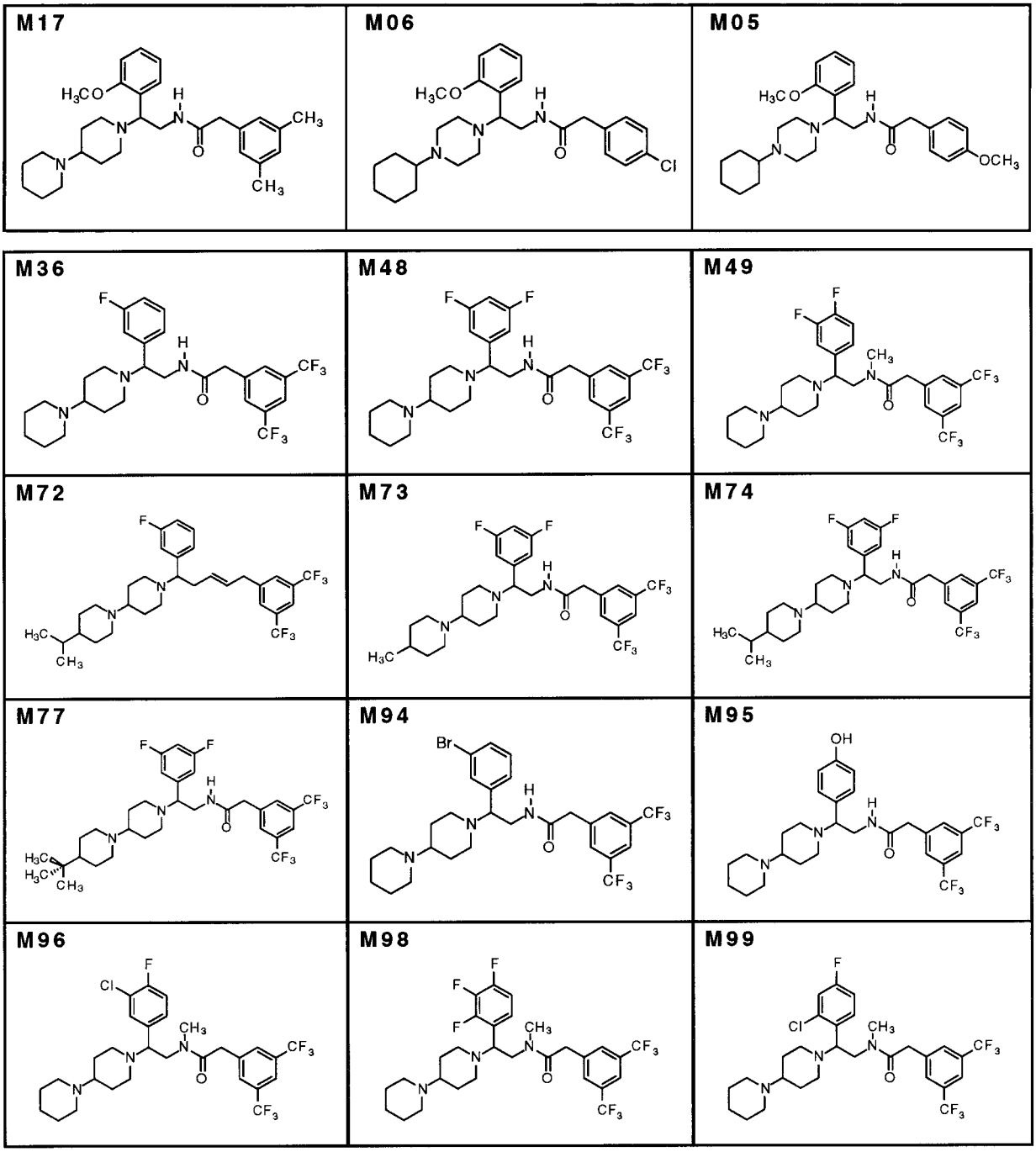

Figure 2. Schematic representation of (top) the 50 ligands of the training set, (middle) the 15 ligands of the test set, and (bottom) the 12 compounds analyzed for predictive purposes.

15 ligands of the test set is 0.51 kcal/mol (2.4 in the IC_{50}) and the maximal individual deviation 1.2 kcal/mol (compound **X13**, 7.2 in the IC_{50}). The analysis of the protomer distribution reveals that the evolution converged at an identical protonation scheme for all antagonist molecules or − when summarized over all conformers − favors this state by a 98:2 ratio, respectively. This state corresponds to the N atom of ring C being protonated or, for the piperazyl-bearing ligands, to the N atom vicinal to ring B. The majority of all compounds adopt a *si* orientation (substituent facing the amide N atom) with respect to ring B: 19 ligands completely, 21 with a preference of more than 95%, 4 with more than 75%, while the remaining 4 adopt this orientation with a preference between 52% and 67%. Seven antagonist molecules (**X20**, **M21**, **M26**, **M11**, **M9M**, **M16**, and **X16**) prefer the *re* (substituent facing the amide O atom) orientation with preferences ranging from 57% to 99%. Ten of the 65 antagonists are not substituted at ring B. Finally, the validity of the model family was assessed by a series of five scramble tests. The resulting predictive r^2 values of −0.363/−0.324/−0.421/−0.464/−0.616 (average: −0.438) demonstrate the sensitivity of the surrogate family toward the experimental IC_{50} data, for which it should establish a QSAR (cf. Figure 4).

On the basis of this surrogate family, the activities of 12 new compounds (cf. Figure 2c) have been predicted. Relative to compound **M09**, the variations include position and type of the substituents at ring B and an

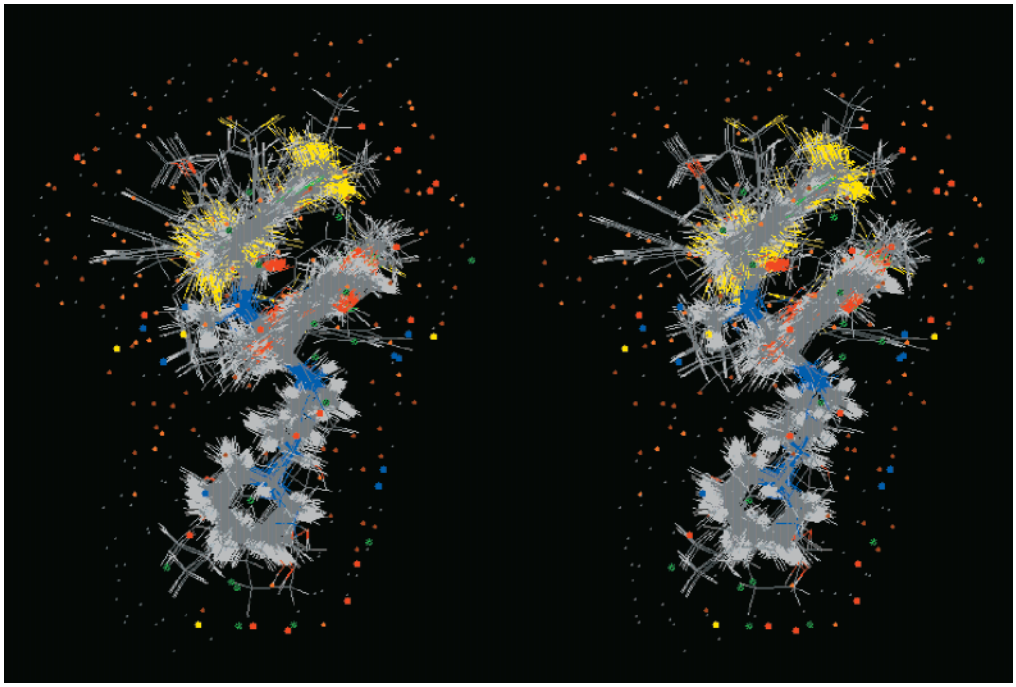

Figure 3. Stereoscopic view of the surrogate for the NK-1 receptor. Color-coding scheme: red, positively charged salt bridge; blue, negatively charged salt bridge; yellow, H-bond donor; green, H-bond acceptor; saddle brown, positively charged hydrophobic; chocolate brown, negatively charged hydrophobic; pink, H-bond flip-flop; gray, neutral hydrophobic. The depicted model corresponds to the most frequently occurring property, averaged over the 500 receptor models.

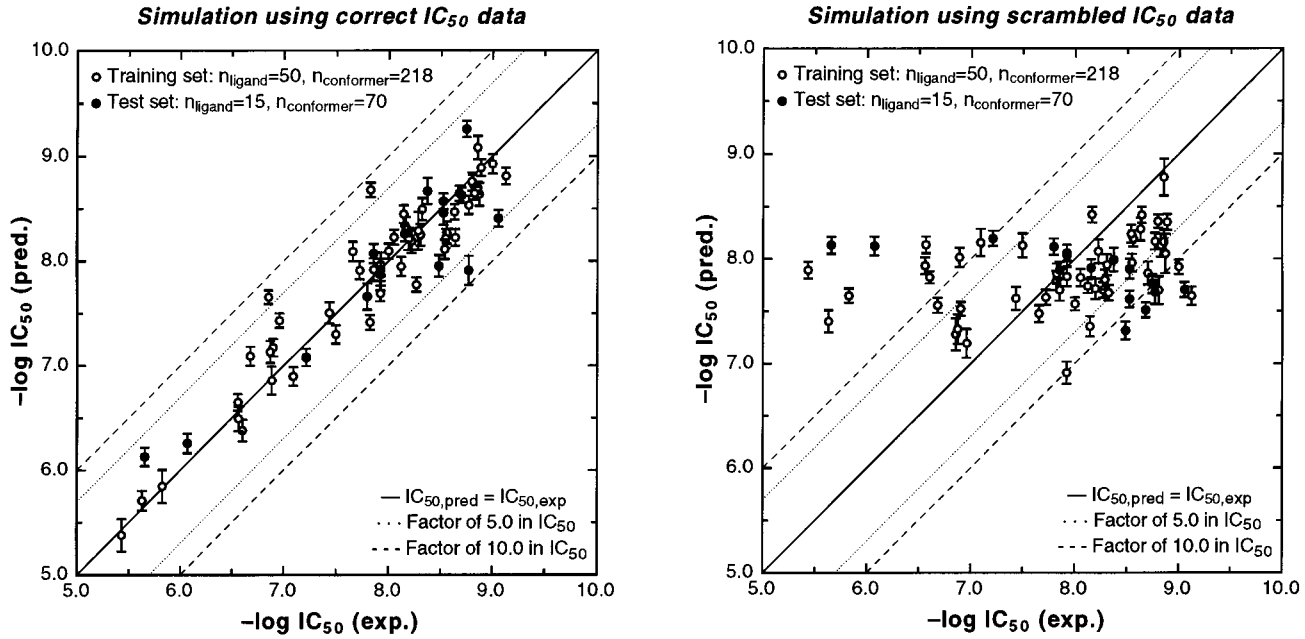

Figure 4. Graphical comparison of experimental and predicted binding affinities for the NK-1 receptor: (left) simulation using correct IC_{50} data; (right) simulation using scrambled IC_{50} data. The error bar corresponds to the variation of the predicted IC_{50} value over the 500 individual receptor models.

apolar link replacing the amide bond, as well as the substituents of ring D (i.e. methyl, isopropyl, *tert*-butyl). Except for ligand **M95** (featuring a 4-hydroxy substitution on ring B, IC_{50} value of 3.2×10^{-8} M), all potential antagonists are predicted with an $IC_{50} < 1.0 \times 10^{-8}$ M: the values range from 9.1×10^{-10} M for compound **M77** to 1.0×10^{-8} M for ligand **M94**. Interestingly, the replacement of the amide moiety by an ethylene bridge in compound **M72** has little effect on the calculated activity (3.9×10^{-9} M). As part of a separate project, four of these compounds (**M36**, **M96**, **M98**, and **M99**) have been synthesized and tested in the meantime at the laboratories of Boehringer Ingelheim (Germany). While the calculated IC_{50} value for compound **M98** (7.7×10^{-9} M) differs by a factor of 4.3 with the experimental value of 1.8×10^{-9} M, the predicted activities for **M36** (8.1×10^{-9} M; exptl 4.6×10^{-9} M), **M96** (2.4×10^{-9} M; exptl 1.7×10^{-9} M), and **M99** (3.2×10^{-9} M; exptl 1.5×10^{-9} M) are in excellent agreement with the experiment.

How can the results obtained with this receptor surrogate be interpreted? It is obvious for this class of

Table 2. Experimental and Calculated IC_{50} Values for the NK-1 Data Set: Training Set (top), Test Set (middle), and Predictions (bottom)[a]

ligand	n_{conf}	IC_{50} (M) expt	IC_{50} (M) calcd	error (factor in IC_{50})	protonation ratio	ligand	n_{conf}	IC_{50} (M) expt	IC_{50} (M) calcd	error (factor in IC_{50})	protonation ratio
M09	4	7.5×10^{-10}	1.6×10^{-9}	2.1	100:0	**M14**	8	1.3×10^{-7}	6.8×10^{-8}	1.9	96:4
X34	4	1.1×10^{-9}	1.2×10^{-9}	1.1	100:0	**X22**	2	1.3×10^{-7}	1.4×10^{-7}	1.1	100:0
X28	4	1.3×10^{-9}	1.3×10^{-9}	1.0	100:0	**M19**	2	1.3×10^{-7}	7.4×10^{-8}	1.8	n/a
M28	4	1.4×10^{-9}	2.3×10^{-9}	1.6	100:0	**X01**	4	1.4×10^{-7}	2.2×10^{-8}	6.4	100:0
X04	4	1.4×10^{-9}	8.3×10^{-10}	1.7	100:0	**X14**	4	2.1×10^{-7}	8.1×10^{-8}	2.6	100:0
X05	4	1.4×10^{-9}	2.0×10^{-9}	1.4	100:0	**M01**	2	2.5×10^{-7}	4.2×10^{-7}	1.7	n/a
X11	8	1.5×10^{-9}	2.3×10^{-9}	1.5	100:0	**M03**	8	2.7×10^{-7}	3.2×10^{-7}	1.2	99:1
M22	4	1.6×10^{-9}	1.8×10^{-9}	1.1	100:0	**M07**	8	2.8×10^{-7}	2.2×10^{-7}	1.3	100:0
X27	4	1.6×10^{-9}	1.7×10^{-9}	1.1	99:1	**X30**	1	1.5×10^{-6}	1.4×10^{-6}	1.1	98:2
X06	4	1.7×10^{-9}	2.9×10^{-9}	1.7	100:0	**M04**	4	2.4×10^{-6}	2.0×10^{-6}	1.2	100:0
M24	2	2.0×10^{-9}	2.4×10^{-9}	1.2	100:0	**M12**	2	3.7×10^{-6}	4.2×10^{-6}	1.1	n/a
M21	4	2.3×10^{-9}	6.0×10^{-9}	2.6	100:0	**M30**	4	8.8×10^{-10}	3.9×10^{-9}	4.4	100:0
M08	4	2.4×10^{-9}	3.4×10^{-9}	1.4	100:0	**X13**	4	1.7×10^{-9}	1.2×10^{-8}	7.1	100:0
M15	4	2.8×10^{-9}	5.4×10^{-9}	1.9	99:1	**X24**	4	1.8×10^{-9}	5.6×10^{-10}	3.2	100:0
M26	4	2.9×10^{-9}	6.1×10^{-9}	2.1	100:0	**X33**	2	2.1×10^{-9}	2.3×10^{-9}	1.1	100:0
X07	4	2.9×10^{-9}	7.8×10^{-9}	2.7	100:0	**X10**	4	3.0×10^{-9}	3.5×10^{-9}	1.2	100:0
M23	4	4.8×10^{-9}	3.2×10^{-9}	1.5	100:0	**X09**	4	3.0×10^{-9}	2.7×10^{-9}	1.1	100:0
M11	8	5.0×10^{-9}	5.6×10^{-9}	1.1	100:0	**M20**	4	3.3×10^{-9}	1.1×10^{-8}	3.3	100:0
X31	8	5.2×10^{-9}	5.2×10^{-9}	1.0	100:0	**M13**	4	4.3×10^{-9}	2.2×10^{-9}	2.0	100:0
M25	2	5.4×10^{-9}	1.7×10^{-8}	3.2	100:0	**M02**	4	7.0×10^{-9}	5.5×10^{-9}	1.3	99:1
X23	8	6.0×10^{-9}	6.5×10^{-9}	1.1	100:0	**X19**	8	1.2×10^{-8}	1.2×10^{-8}	1.0	100:0
X15	4	6.4×10^{-9}	6.2×10^{-9}	1.0	100:0	**X32**	4	1.4×10^{-8}	8.5×10^{-9}	1.6	100:0
M27	4	6.9×10^{-9}	4.7×10^{-9}	1.5	100:0	**X17**	8	1.6×10^{-8}	2.2×10^{-8}	1.4	100:0
M10	4	7.2×10^{-9}	3.6×10^{-9}	2.0	99:1	**M17**	4	6.1×10^{-8}	8.3×10^{-8}	1.4	100:0
X20	4	7.6×10^{-9}	1.1×10^{-8}	1.4	100:0	**M06**	4	8.5×10^{-7}	5.5×10^{-7}	1.5	97:3
X02	4	8.9×10^{-9}	5.9×10^{-9}	1.5	100:0	**M05**	8	2.2×10^{-6}	7.5×10^{-7}	2.9	100:0
X21	4	1.0×10^{-8}	8.1×10^{-9}	1.2	100:0						
X08	4	1.2×10^{-8}	1.4×10^{-8}	1.2	100:0	**36**	4	4.6×10^{-9}	8.1×10^{-9}	1.8	100:0
X26	4	1.2×10^{-8}	1.1×10^{-8}	1.1	100:0	**48**	2	–	4.1×10^{-9}	–	100:0
X12	4	1.2×10^{-8}	2.0×10^{-8}	1.7	100:0	**49**	4	–	4.3×10^{-8}	–	100:0
X25	2	1.4×10^{-8}	1.2×10^{-8}	1.2	100:0	**72**	4	–	3.9×10^{-9}	–	100:0
M9M	4	1.5×10^{-8}	2.1×10^{-9}	7.1	100:0	**73**	2	–	1.4×10^{-9}	–	100:0
M18	4	1.5×10^{-8}	3.9×10^{-8}	2.6	100:0	**74**	2	–	1.1×10^{-9}	–	100:0
M16	4	1.9×10^{-8}	1.2×10^{-8}	1.6	100:0	**77**	2	–	9.1×10^{-10}	–	100:0
M29	12	2.2×10^{-8}	8.1×10^{-9}	2.7	100:0	**94**	4	–	1.0×10^{-8}	–	100:0
X18	2	3.2×10^{-8}	5.0×10^{-8}	1.6	100:0	**95**	4	–	3.2×10^{-8}	–	100:0
X16	4	3.7×10^{-8}	3.1×10^{-8}	1.2	100:0	**96**	4	1.7×10^{-9}	2.4×10^{-9}	1.4	100:0
X29	2	8.1×10^{-8}	1.3×10^{-7}	1.6	100:0	**98**	4	1.8×10^{-9}	7.7×10^{-9}	4.3	100:0
X03	8	1.1×10^{-7}	3.7×10^{-8}	3.4	100:0	**99**	4	1.5×10^{-9}	3.2×10^{-9}	2.1	100:0

[a] The protonation ratio upper:lower N atom corresponds to the scheme in Figure 1a. n/a, does not apply for three compounds bearing only a single amine function.

NK-1 antagonists that a polar substitution at ring B (e.g. the hydroxyl group of ligand **M95**) reduces the intrinsic activity because of the higher desolvation energy (cf. eq 1). Modifications of the halide substitution pattern on ring B (F or mixed F/Cl patterns, e.g. **M77**) combined with small, apolar substituents at ring D would seem to be most promising due to an optimal balance between a low desolvation energy and a high intrinsic affinity (cf. eq 1). The bis-trifluoro substitution of ring A is certainly a key to high activity. Less obvious is the role of the amide N atom (which can be highly active in both the methylated and protonated states) as well as changes associated with ring D. Here, the training set might not yet be representative enough to allow for safe predictions: ligand **M9M**, for example, is predicted 7.1 times more active than toward the true biological receptor. Compared with an earlier study[27] using a subset of these compounds (31 ligands, single-ligand representation: 3D-QSAR), it may be concluded that 4D-QSAR can handle large data sets with substantial variability in both conformation and protonation status and still produce more accurate results.

Conclusions

In absence of an experimentally determined receptor structure, 4D-QSAR techniques provide an elegant approach to the estimation of free energies of ligand binding. The *Quasar* concept developed at our laboratory not only allows for the representation of the ligand molecules by an ensemble of conformation, orientations, and protonation states but also takes local induced fit and H-bond flip-flop into account. This approach has been used to predict the IC_{50} values of NK-1 antagonists (featuring both conformational flexibility as well as multiple protonation states). The results indicate that the use of 4D-QSAR significantly reduces the bias associated with the ligand alignment. Moreover, the selection protocol demonstrates that the technique is capable of identifying a small number of active conformations and does not prefer a larger selection of lesser-contributing entities.

The challenge of the NK-1 system presented in this account was to allow for both different conformation and protonation states. A previous study included the aryl hydrocarbon receptor[29] where the 131 investigated dibenzodioxin, dibenzofuran, biphenyl, and polyaromatic hydrocarbon molecules can adopt up to four different orientations with respect to the binding pocket. An ongoing study includes the benzodiazepine/$GABA_A$ receptor where some of the ligands are provided as racemic mixtures. Again, the *Quasar* concept was

capable to quantitatively identify the correct enantiomer,[55] demonstrating the potential of 4D-QSAR.

Acknowledgment. The authors are indebted to Prof. James P. Snyder (Emory University, Atlanta, GA), Prof. Gerd Folkers (Department of Pharmacy, ETH Zürich, Switzerland), and Dr. Herbert Köppen (Boehringer Ingelheim, Germany) for most valuable discussions. Financial support from the Margaret and Francis Fleitmann Foundation (Luzern, Switzerland) and the Foundation for Animal-free Research (Zürich, Switzerland) is gratefully acknowledged.

References

(1) Regoli, D.; Boudon, A.; Fauchère, J.-L. Receptors and antagonists for substance P and related peptides. *Pharmacol. Rev*. **1994**, *46*, 551−599.
(2) Quartera, L.; Maggi, C. A. The tachykinin NK-1 receptor. Part I: Ligands and mechanisms of cellular activation. *Neuropeptides* **1997**, *31*, 537−563.
(3) von Euler, U. S.; Gaddum, J. H. An unidentified depressor substance in certain tissue extracts. *J. Physiol. (London)* **1931**, *72*, 74−87.
(4) Maggi, C. A.; Schwartz, T. W. The dual nature of the tachykinin NK-1 receptor. *Trends Pharmacol. Sci.* **1997**, *18*, 351−355.
(5) Takeuchi, Y.; Shands, E. F. B.; Beusen, D. D.; Marshall, G. R. Derivation of a three-dimensional pharmacophore model of substance P antagonists bound to the NK-1 receptor. *J. Med. Chem*. **1998**, *41*, 3609−3623.
(6) Ladduwahetty, T.; Baker, R.; Cascieri, M. A.; Chambers, M. S.; Haworth, K.; Keown, L. E.; MacIntyre, D. E.; Metzger, J. M.; Owen, S.; Rycroft, W.; Sadowsky, S.; Seward, E. M.; Shepheard, S. L.; Swain, C. J.; Tatters, F. D.; Watt, A. P.; Williamson; D. W.; Hargreaves, R. J. N-Heteroaryl-2-phenyl-3-(benzyloxy)-piperidines: A novel class of potent orally active human NK-1 antagonists. *J. Med. Chem*. **1996**, *39*, 2907−2914.
(7) Baldwin, J. M. Structure and function of receptors coupled to G proteins. *Curr. Opin. Cell. Biol*. **1994**, *6*, 180−190.
(8) Turcatti, G.; Zoffman, S.; Lowe, J. A.; Drozda, S. E.; Chassaing, G.; Schwartz, T. W.; Chollet, A. Characterization of non-peptide antagonist and peptide agonist binding sites of the NK1-receptor with fluorescent ligands. *J. Biol. Chem*. **1997**, *272*, 21167−21175.
(9) Henderson, R.; Baldwin, J. M.; Ceska, T. A.; Zemlin, F.; Beckmann, E.; Downing, K. H. The structure of bacteriorhodopsin. *J. Mol. Biol*. **1990**, *213*, 899−929.
(10) Edman, K.; Nollert, P.; Royant, A.; Belrhali, H.; Pebay-Peyroula, E.; Hajdu, J.; Neutze, R.; Landau, E. M. High-resolution X-ray strucuture of an early intermediate in the Bacteriorhodopsin photocycle. *Nature* **1999**, *401*, 6755.
(11) Fong, T. M.; Cascieri, M. A.; Yu, H.; Bansal, A.; Swain, C.; Strader, C. D. Amino-aromatic interaction between histidine 197 of the neurokinin-1 receptor and CP-96,345. *Nature* **1993**, *362*, 350−353.
(12) Fong, T. M.; Yu, H.; Cascieri, M. A.; Underwood, D.; Swain, C. J.; Strader, C. D. The role of histidine 265 in antagonist binding to the neurokinin-1 receptor. *J. Biol. Chem*. **1994**, *269*, 2728−2732.
(13) Fong, T. M.; Yu, H.; Cacieri, M. A.; Underwood, D.; Swain, C. J.; Strader, C. D. Interaction of glutamine 165 in the fourth transmembrane segment of the human neurokinin-1 receptor with quinuclidine antagonists *J. Biol. Chem*. **1994**, *269*, 14957−14961.
(14) Cascieri, M. A.; Fong, T. M.; Strader, C. D. Identification of critical functional groups within binding pockets of G-protein-coupled receptors. *Drugs Future* **1996**, *21*, 521−527.
(15) Sisto, A.; Bonelli, F.; Centini, F.; Fincham, C. I.; Potier, E.; Monteagudo, E.; Lombardi, P.; Arcamone, F.; Goso, C.; Manzini, S.; Giolitti, A.; Maggi, C. A.; Venanzi, M.; Pispisa, B. Synthesis and biological evaluation of novel NK-1 tachykinin receptor antagonists: The use of cycloalkyl amino acids as a template. *Biopolymers* **1995**, *36*, 511−524.
(16) Horwell, D. C. (Warner-Lambert). Alpha-substituted polypetides having therapeutical activity. United States Patent No. WO 92 19254, 1992.
(17) Snyder, J. P.; Rao, S. N.; Koehler, K. F.; Vedani, A. Pseudoreceptors. In *3D QSAR in Drug Design*; Kubinyi, H., Ed.; ESCOM Science Publishers: Leiden, 1993; pp 336−354.
(18) Vedani, A.; Zbinden, P.; Snyder, J. P.; Greenidge, P. A. Pseudoreceptor modeling: The construction of three-dimensional receptor surrogates. *J. Am. Chem. Soc*. **1995**, *117*, 4987−4994.
(19) Zbinden, P.; Dobler, M.; Folkers, G.; Vedani, A. PrGen: Pseudoreceptor modeling using receptor-mediated ligand alignment and pharmacophore equilibration. *Quant. Struct.-Act. Relat*. **1998**, *17*, 122−130.
(20) Montgomery, J. A.; Secrist, J. A., III. PNP inhibitors. *Perspect. Drug Discov. Des*. **1994**, *2*, 205−220.
(21) Kubinyi, H. QSAR and 3D QSAR in drug design. 1. Methodology. *Drug Discovery Today* **1997**, *2*, 457−467.
(22) Kubinyi, H. QSAR and 3D QSAR in drug design. 2. Applications and problems. *Drug Discovery Today* **1997**, *2*, 538−546.
(23) Kubinyi, H.; Folkers, G.; Martin, Y. C. QSAR: Current state, scope, and limitations. *Perspect. Drug Discovery Des*. **1998**, *12*, 3−23.
(24) Hopfinger, A. J.; Wang, S.; Tokarski, J. S.; Jin, B. Q.; Albuquerque, M.; Madhav, P. J.; Duraiswami, C. Construction of 3D-QSAR models using 4D-QSAR analysis formalism. *J. Am. Chem. Soc*. **1997**, *119*, 10509−10524.
(25) So, S. S.; Karplus, M. Three-dimensional quantitative structure−activity relationships from molecular similarity matrixes and genetic neural networks. *J. Med. Chem*. **1997**, *40*, 4347−4359.
(26) Sprague, P. W.; Hoffmann, R. Catalyst pharmacophore models and their utility as queries for searching 3D databases. In *Computer-Assisted Lead Finding and Optimization*; van de Waterbeemd, H., Testa, B., Folkers, G., Eds.; VCH Weinheim: Germany, 1997; pp 223−240.
(27) Vedani, A.; Dobler, M.; Zbinden, P. Quasi-atomistic receptor surface models: A bridge between 3-D QSAR and receptor modeling. *J. Am. Chem. Soc*. **1998**, *120*, 4471−4477.
(28) Vedani, A.; McMasters, D. R.; Dobler, M. Multi-conformational ligand representation in 4D-QSAR: Reducing the bias associated with ligand alignment. *Quant. Struct.-Act. Relat*. **2000**, *19*, 149−161.
(29) Vedani, A.; Dobler, M. Multidimensional QSAR in drug research: Predicting binding affinities, toxicity, and pharmacokinetic parameters. In *Progress in Drug Research*; Jucker, E., Ed.; Birkhäuser: Basel/Boston/Berlin, 2000; pp 105−135.
(30) Hahn, M. Receptor surface models. 1. Definition and construction. *J. Med. Chem*. **1995**, *38*, 2080−2090.
(31) Srivastava, S.; Richardson, W. W.; Bradley, M. P.; Crippen, G. Three-dimensional receptor modeling using distance geometry and Voronoi polyhedra. In *3D-QSAR in drug design: Theory, Methods and Applications*; Kubinyi, H., Ed.; ESCOM: Leiden, 1993; pp 80−116.
(32) Walters, D. E.; Hinds, R. M. Genetically evolved receptor models: A computational approach to construction of receptor models. *J. Med. Chem*. **1994**, *37*, 2527−2536.
(33) Hahn, M.; Rogers, D. Receptor surface models. 2. Application to quantitative structure−activity studies. *J. Med. Chem*. **1995**, *38*, 2091−2102.
(34) Ekins, S.; Bravi, G.; Binkley, S.; Gillespie, J. S.; Ring, B. J.; Wikel, J. H.; Wrighton, S. A. Three- and four-dimensional-quantitative structure activity relationship (3D/4D-QSAR) analyses of CYP2C9 inhibitors. *Drug. Metab. Dispos*. **2000**, *28*, 994−1002.
(35) Robinson, A. U.; Winn, P. J.; Lyne, P. D.; Richards, W. G. Self-organizing molecular field analysis: A tool for structure−activity studies. *J. Med. Chem*. **1999**, *42*, 573−583.
(36) The actual field excerted by all atoms of a given ligand molecule onto its envelope is determined using a nondirectional force field as, at this point, no atomic properties are deposited on the surface.
(37) We plan to address this problem soon by including an additional degree of freedom into the *Quasar* algorithm, allowing for a genetically controlled induced fit. In this 5D-QSAR approach, the target receptor will be represented by an ensemble of differently shaped binding pockets.
(38) Rogers, D.; Hopfinger, A. J. Genetic function approximation to generate a family of QSAR equations using genetic algorithms. *J. Chem. Inf. Comput. Sci*. **1994**, *34*, 854−866.
(39) Blaney, J. M.; Weiner, P. K.; Dearing, A.; Kollman, P. A.; Jorgensen, E. C.; Oatley, S. J.; Burridge, J. M.; Blake. J. F. Molecular mechanics simulation of protein−ligand interactions: Binding of thyroid analogues to prealbumin. *J. Am. Chem. Soc*. **1982**, *104*, 6424−6434.
(40) Still, W. C.; Tempczyk, A.; Hawley, R. C.; Hendrickson, T. Semianalytical treatment of solvation for molecular mechanics and dynamics. *J. Am. Chem. Soc*. **1990**, *112*, 6127−6129.
(41) Searle, M. S.; Williams, D. H. The cost of conformational order: Entropy changes in molecular associations. *J. Am. Chem. Soc*. **1992**, *114*, 10690−10697.
(42) Vedani, A.; Huhta, D. W. A new force field for modeling metalloproteins. *J. Am. Chem. Soc*. **1990**, *112*, 4759−4767.
(43) As a virtual particle (VP) in a quasi-atomistic approach has no bonding partners (i.e. unlike functional groups of real molecules it bears no lone pairs), we apply a reduced function to determine the nonelectrostatic contribution to the H-bond energy involving a VP: For the constellation Don-H···VP, we correct for nonlinearity of the Don-H···VP angle (compulsory assuming a perfect directionality at the VP). For the arrangement Acc···VP, we correct for the deviation of the virtual hydrogen bond from the closest lone pair at the acceptor fragment (angle LP−Acc···VP) and assume a perfect linearity of the hydrogen bond. Derivation

and calibration of the directional function for H-bond interactions is described in refs 18 and 42.
(44) Schnorrenberg, G.; Dollinger, H.; Esser, F.; Briem, H.; Jung, B.; Speck, G. Preparation of arylglycinamide derivatives as tachykinin antagonists. Ger. Offen. 1996, 29 pp (patent written in German).
(45) Chang, G.; Guida, W. C.; Still, W. C. An internal coordinate Monte Carlo method for searching conformational space. *J. Am. Chem. Soc.* **1989**, *111*, 4379−4386.
(46) Mohamadi, F.; Richards, N. G. J.; Guida, W. C.; Liskamp, R.; Lipton, M.; Caufield, C.; Chang, G.; Hendrickson, T.; Still, W. C. MacroModel − An integrated software system for modeling organic and bioorganic molecules using molecular mechanics. *J. Comput. Chem.* **1990**, *11*, 440−467.
(47) Ponder, J. W.; Richards, F. M. An efficient Newton-like method for molecular mechanics ernergy minimization of large molecules *J. Comput. Chem.* **1987**, *8*, 1016−1024.
(48) Weiner, S. J.; Kollmann, P. A.; Case, D. A.; Singh, U. C.; Ghio, C.; Alagona, G.; Profeta, S., Jr.; Weiner, P. A new force field for molecular-mechanical simulation of nucleic acids and proteins. *J. Am. Chem. Soc.* **1984**, *106*, 765−784.
(49) Besler, B. H.; Merz, J., K. M.; Kollman, P. A. Atomic charges derived from semiempirical methods *J. Comput. Chem.* **1990**, *11*, 431−439.
(50) Stewart, J. J. P. MOPAC − A semiempirical molecular orbital program *J. Comput.-Aided Mol. Des.* **1990**, *4*, 1−105.
(51) Distributed by QCPE, University of Indiana, Bloomington, IN; Program No. 455.
(52) Dewar, M. J. S.; Thiel, W. Ground states of molecules. The MNDO method. Approximations and parameters. *J. Am. Chem. Soc.* **1977**, *99*, 4899−4907.
(53) This option in *Quasar* allows for the exclusion of bulky ligands with low intrinsic binding energy[54] with respect to the generation of the mean envelope.
(54) The intrinsic binding affinity (IBE) approximates the enthalpic contribution to the ligand−receptor energy: IBE $\approx \Delta G°_{exp} + T\Delta S_{bdg} + E_{solv,lig}$.
(55) Vedani, A.; Dobler, M. The benzodiazepine/$GABA_A$ receptor: modeling racemic mixtures in 4D-QSAR. *J. Am. Chem. Soc.*, in preparation.

JM000986N